KENTUCKY GEOLOGICAL SURVEY

Report of Investigations 1, Series XIV, 2025

Evaluating the Physics-Based Slope Stability Program PISA-m at a Regional Scale

Hudson J. Koch, William C. Haneberg, Matthew M. Crawford,
Jason M. Dortch, and Meredith L. Swallom

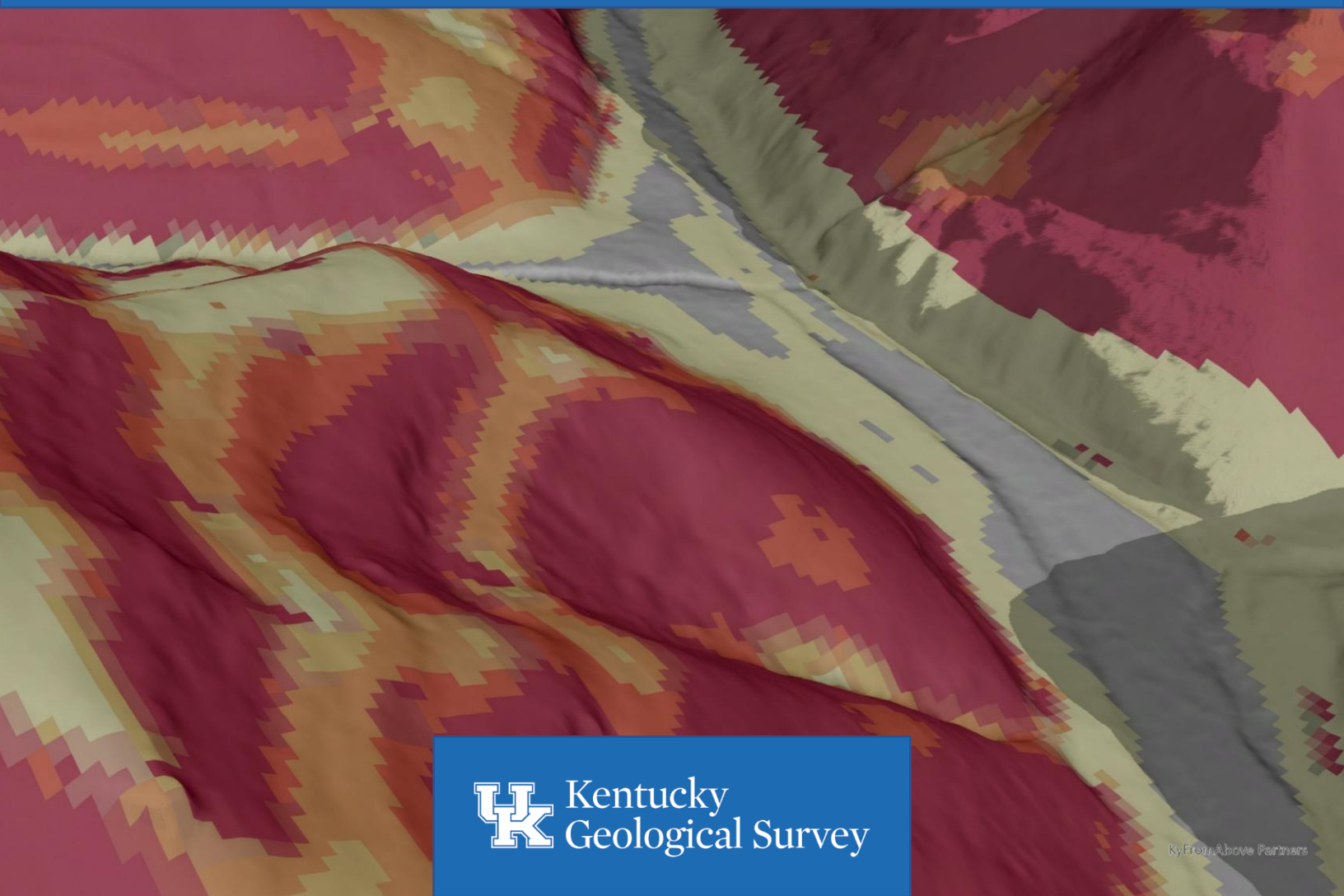

Kentucky Geological Survey

KyFromAbove Partners

Kentucky Geological Survey
Michael McGlue, State Geologist and Director
University of Kentucky, Lexington

Evaluating the Physics-Based Slope Stability Program PISA-m at a Regional Scale

by Hudson J. Koch[1], William C. Haneberg[2], Matthew M. Crawford[1], Jason M. Dortch[1], and Meredith L. Swallom[1]

[1]Kentucky Geological Survey, University of Kentucky
[2]Geological and Geohazards Consultant

Suggested Citation:

Koch, H.J., Haneberg, W.C., Crawford, M.M., Dortch, J.M., and Swallom, M.L., 2025, Evaluating the physics-based slope stability program PISA-m at a regional scale: Kentucky Geological Survey, ser. 14, Report of Investigations 1, 22 p.

Our Mission

The Kentucky Geological Survey is a state-supported research center and public resource within the University of Kentucky. Our mission is to support sustainable prosperity of the commonwealth, the vitality of its flagship university, and the welfare of its people. We do this by conducting research and providing unbiased information about geologic resources, environmental issues, and natural hazards affecting Kentucky.

Technical Level

General Intermediate Technical

Statement of Benefit to Kentucky

Computer models based on topography, soil properties, and water levels in hillsides can help identify areas susceptible to landslides triggered by rainstorms or human activity like logging, mining, or construction. This study compares results from one computer model, called PISA-m, using different kinds of soil property information to known landslide locations in parts of eastern Kentucky to evaluate the effectiveness of the model.

Evaluating the Physics-Based Slope Stability Program PISA-m at a Regional Scale

Hudson J. Koch, William C. Haneberg, Matthew M. Crawford, Jason M. Dortch, and Meredith L. Swallom

Abstract

Physics-based landslide modeling can be difficult and data-intensive. Generating high-quality and practical map results is often not feasible outside of small, thoroughly characterized study areas. Using the physics-based program Probabilistic Infinite Slope Analysis (PISA-m), users can perform expedient assessments of landslide hazard over large study areas where comprehensive geotechnical data may be lacking, but other data inputs are robust. PISA-m uses an infinite slope equation and spatial layers, such as a digital elevation model (DEM), a lidar-derived forest cover layer, and a soil map, to calculate the probability that the factor of safety (or *FS*) for an area will be less than or equal to one. Factor of safety values less than or equal to one often infer slope instability. This investigation considers two landslide inventories, one reflecting the assumed background climatic conditions seen over a decade and the other gathered following an extreme rainfall event. These two weather scenarios were approximated with parameter specifications and used over four models based on different soil unit inputs: shale beds with alluvium and colluvium, 1:24,000 scale bedrock formations, United Soil Classification System (USCS) distributions with geotechnical values derived from drilling reports, and USCS distributions with generalized geotechnical values. Model results were symbolized as five susceptibility groups based on equal intervals of the probability of $FS \leq 1$. The model results were compared to landslides that post-date the lidar DEM and non-landslide locations to evaluate the program's accuracy as a regional landslide susceptibility tool. PISA-m results indicating a high probability (0.50–1.0) of $FS \leq 1$ around a landslide were considered true positives, while lower probabilities (0–0.50) for non-landslide areas were considered true negatives. Model accuracies varied across the models and study areas, averaging 78% for the background climatic conditions proxy and 82% for the extreme rainfall event area, with the best model accuracy of 84% for the shale bed case in the extreme event specifications. While these practical, first-order landslide susceptibility model results are promising, these outcomes rely on effective use of high-resolution input data and expert knowledge of ground characterization to bolster the lack of precise geotechnical descriptions.

Introduction

In Kentucky, landslides are estimated to directly cost $20 million a year (Crawford, 2014; Overfield et al., 2015), with indirect costs likely greater. To assist in landslide hazard avoidance and mitigation, landslide susceptibility models are created. Approaches for susceptibility modeling are broadly classified as either statistics based or physics based (Soeters and Westen, 1996; Crozier and Glade, 2005). Statistical models typically leverage geomorphic conditioning factors to predict landslide probability (Reichenbach et al., 2018). Alternatively, physics-based models couple geotechnical parameters of the soil and rock with slope stability and hydrological relationships to calculate metrics such as factor of safety based on the force balance acting on the slope (Formetta et al., 2016). Recent literature suggests that these distinct modeling approaches can be combined as two-step assessments, leveraging statistical models as inputs for physics-based models and vice-versa (Khabiri et al., 2023). Furthermore, these models can be classified as either deterministic or probabilistic, with empirical and rational subdivisions for both model classes. Deterministic models have distinguishable, set outcomes produced using known physical parameters and either rational governing equations or empirical relationships, whereas probabilistic models are used to address random behavior in any of these physical parameters (Haneberg, 2000). The probabilistic modeling approach is suitable for landslide susceptibility analysis when a rational equation can be used to describe the slope failure mechanics, but precise input variable characteristics are not well known.

Statistical landslide susceptibility models are often used in contemporary landslide susceptibility studies (Reichenbach et al., 2018; Crawford et al., 2021). These approaches often require an inventory dataset, advanced GIS technology, and machine learning tools. In addition, models created from these approaches are often considered “black boxes,” making them unwieldy and difficult for researchers and end users to interpret. On the other hand, physics-based slope stability models are more interpretable and have been created for a wide variety of use cases (Montgomery and Dietrich, 1994; Wu and Sidle, 1995; Pack et al., 1998; Baum et al., 2008; Capparelli and Versace, 2011). However, many physics-based modeling programs require comprehensive geotechnical parameters, which can limit assessments to small watershed-scale investigations (Soeters and Westen, 1996). Most of these models do not account for parameter uncertainty and variability, with only a few exceptions (Pack et al., 1998; Haneberg, 2007). While the geotechnical parameter requirement exists universally in physics-based models, calculating probabilities using a range of geotechnical parameters can both account for natural variability inherent in the landscape and address the lack of precise geotechnical values. Despite these potential limitations, physics-based models with landslide susceptibility presented in engineering terms like factor of safety are easy to interpret and understand, making them appealing to a wide variety of mitigation managers and engineers. The additional benefit of selecting a probabilistic and physics-based modeling approach over a strictly deterministic approach is the ability to approximate the probability of factor of safety results as landslide susceptibility models. The aim of this study was to assess limited geotechnical parameters within the modeling program Probabilistic Infinite Slope Analysis (PISA-m). Additionally, PISA-m was evaluated for practicality at a regional scale, and the inherent challenges of parameter uncertainty were addressed. To evaluate model accuracy, PISA-m results were compared to known landslide occurrences from two landslide point inventories.

Study Area

The primary study area, referred to as location 1, was defined as a band stretching across portions of four eastern Kentucky counties in which a rapid reconnaissance landslide inventory was performed following the July 2022 extreme rainfall and flooding event (Crawford et al., 2023; NWS, 2023; Fig. 1). The area comprising location 1 was defined by the extent of an extreme precipitation event in July 2022 and covers ~1250 km^2 (480 mi^2) in Breathitt, Knott, Owsley, and Perry counties.

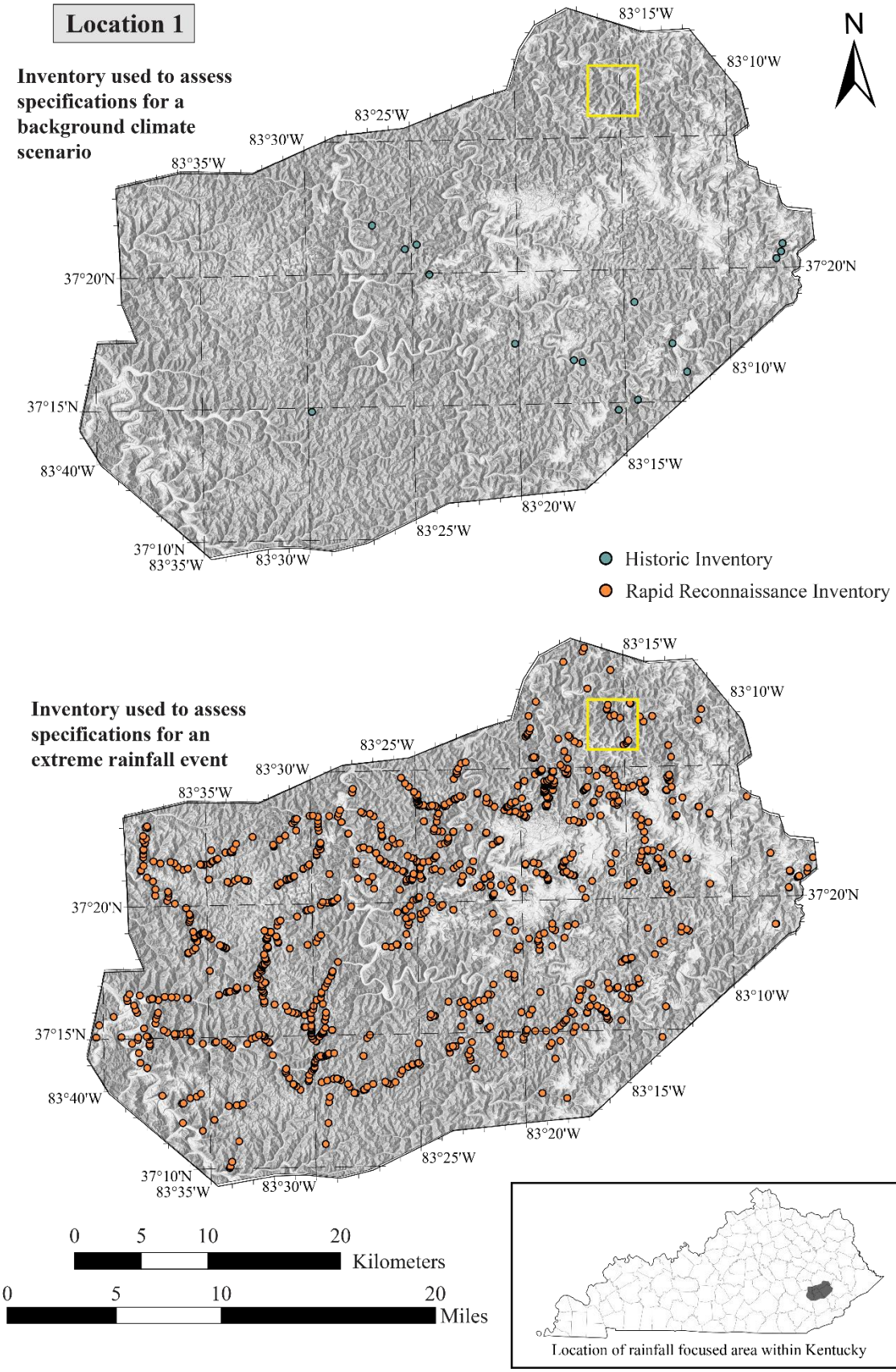

Figure 1. Location 1, defined as the approximate area affected by an extreme rainfall event in July 2022. For this location, results were generated with parameter specifications that approximated background climatic conditions and utilized a recorded historic landslide inventory for assessment (Crawford, 2022). Additionally, a second parameter specification approximated an extreme rainfall event and used the rapid reconnaissance landslide inventory corresponding to the July 2022 rainfall event (Crawford et al., 2023). Yellow squares denote insets used in Figures 4, 6, and 7.

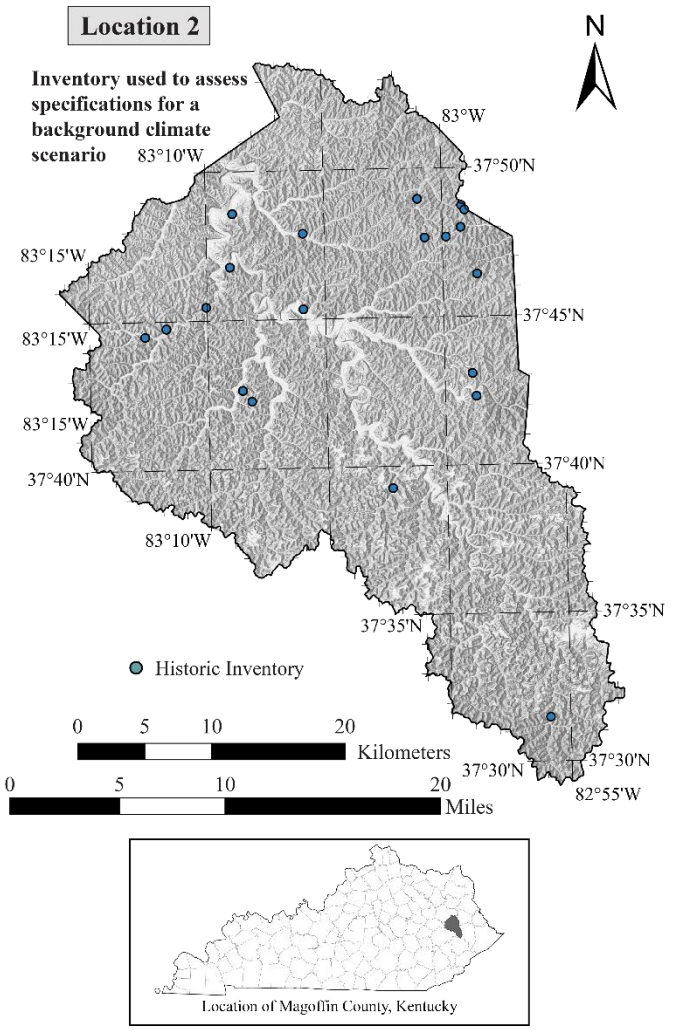

Figure 2. Location 2, the study area defined as the extent of Magoffin County, Kentucky. For this location, results were generated with a parameter specification that modeled background climatic conditions and used a historic landslide inventory (Crawford, 2022).

Location 1 has an average slope of 21.8°. This area was selected based on known landslide occurrences and the availability of landslide inventories with known failure dates that occurred after the collection of digital elevation model (DEM) ground data. A second study area was included to add to the background climatic condition landslides counts and test PISA-m's utility at the county scale. This study area, known as location 2, was defined as the extent of Magoffin County (Fig. 2), which was selected in part because of the digitized landslide inventory present in the area (Crawford et al., 2021). Location 2 covers ~881 km^2 (310 mi^2) and has an average slope of 21.4°. The topography of both study areas is characterized by steep, narrow, sinuous valleys carved by unglaciated, dendritic fluvial systems. Both areas have undergone varying degrees of surface and underground coal mining, logging, and infrastructure construction. Bedrock geology in both areas comprises nearly flat-lying Middle Pennsylvanian sedimentary strata, specifically sandstones, limestones, siltstones, shale, coal seams, and underclays (McDowell, 1986; Greb et al., 2009). Marine and organic shale beds exist in the study areas and have been mapped as distinct rock units. These shale beds are noteworthy and provide insight into landslide occurrence, as shale, coal, and underclay beds are known to weather easily (Outerbridge, 1987; Crawford, 2014; Chapella et al., 2019). The bedrock is overlain by colluvium of variable thickness, in which deposition is primarily controlled by mass wasting processes such as landslides (McDowell, 1986). Landslides in the colluvium are typically thin (less than 3 m deep) translational or thicker rotational landslides. Both translational and rotational landslides have the potential to develop into debris flows (Crawford, 2014; Crawford et al., 2021).

Methods

PISA-m

PISA-m is a physics-based probabilistic slope stability modeling program that utilizes the first-order, second-moment (FOSM) implementation of the infinite slope equation developed by the U.S. Department of Agriculture Forest Service for the LISA and DLISA programs (Hammond et al., 1992; Haneberg, 2007). The infinite slope equation is itself an approximation of slope failure mechanics. The infinite slope equation assumes an infinitely long slope plane with a parallel failure surface; specifically, the length of the landslide is much larger than the thickness to the failure plane (Dai and Lei, 2025). This approximation does not translate well to thicker movements or complex failure geometries; however, most landslides in eastern Kentucky are thin, translational slope failures (Crawford et al., 2021), and the infinite slope equation is therefore a reasonable approximation. The infinite slope factor of safety equation used in PISA-m (Hammond et al., 1992; Haneberg, 2004, 2007) is

$$FS = \frac{c_r + c_s + [q_t + \gamma_m D + \ \gamma_{sat} - \gamma_w - \gamma_m \ H_w D] \cos^2 \beta \tan \phi}{[q_t + \gamma_m D + \ \gamma_{sat} - \gamma_m \ H_w D] \sin \beta \cos \beta}, \quad (1)$$

where *FS* corresponds to a factor of safety value, c_r is the cohesive strength from tree roots in Pa, c_s is the cohesive strength of soil in Pa, q_t is a uniform surcharge exerted by vegetation in Pa, γ_m is the unit weight of moist soil in N/m^3, γ_{sat} is the unit weight of saturated soil in N/m^3, γ_w is the unit weight of water, *D* is the thickness of soil above slip surface in m, H_w is the unitless height of the phreatic surface (relative to the water table) above slip surface, β is the slope angle in degrees, and ϕ is the angle of internal friction in degrees.

Infinite slope models assume that 1) the failure plane is parallel to the topographic and phreatic surfaces, 2) the failure plane extends infinitely in all directions, and 3) there is a single soil layer with uniform properties (Hammond et al., 1992). Despite these assumptions, infinite slope models and PISA-m are useful reconnaissance tools for characterizing the landslide hazard in an area.

PISA-m uses mean values of the parameters in Equation 1 to calculate a mean *FS* value,

$$\overline{FS} = FS\ x\ , \tag{2}$$

and a truncated Taylor series approximation of the *FS* variance (the square of the standard deviation; Haneberg, 2004, 2007),

$$s_F^2 = \sum_i \left(\frac{\partial FS}{\partial x_i}\right)_{\overline{x}}^2 s_{x_i}^2. \tag{3}$$

Once the mean and variance have been calculated, probability of $FS \leq 1$ (Prob[$FS \leq 1$]) is determined by calculating the value of the cumulative distribution function of *FS* at a value of $FS = 1$, where *FS* is assumed to be log-normally distributed. Haneberg (2004, 2012) evaluated the validity of an a priori log-normal assumption for FOSM infinite slope models and found the log-normal assumption to work well in most situations. The FOSM approach implemented by PISA-m assumes that the input parameters are uncorrelated; however, correlation among parameters can be included in FOSM approximations (Haneberg, 2016). Because the FOSM approximation is non-iterative (as opposed to computationally intensive Monte Carlo simulations and other iterative algorithms), PISA-m can generate usefully reliable results in a fraction of the time that would be required by an iterative simulation. This speed and computational simplicity are useful when working with large, high-resolution DEMs over regional scales.

Model Requirements

PISA-m requires a DEM, map layers representing soils and forest cover, and a plain text parameter file. In this study, the DEM provided the basis for slope angle calculation, and the soils and forest cover map layers provided detailed spatial extents for the geotechnical data. The parameters file was used to assign model settings and geotechnical parameters (cohesions, internal angle of friction, surcharge, soil depth, pore pressure coefficient, and unit weights) to the soils units present in the map layers. The parameters file listed the geotechnical values that were assigned to the spatial extents defined by the input soils and forest cover layers, along with a probability distribution for each variable. The parameters file can also be used to enable slope stability calculations based on seismic activity, similar to Newmark analysis (Newmark, 1959; Haneberg, 2004).

Data Distributions

Using the FOSM probabilistic method, PISA-m can effectively account for uncertainty by allowing the user to select the most appropriate data distributions for each geotechnical parameter. PISA-m is equipped with several data distribution types; those relevant to this study and discussion are normal, uniform, and extreme value type I (or Gumbel) distributions. These distributions and other are described in Haneberg (2007). Parameter values used in PISA-m can also be scalar constants, in which case there is no distribution assigned.

Model Cases

As PISA-m has the ability to compute Prob[$FS \leq 1$] quickly over large datasets and account for imprecise geotechnical values and the uncertainty intrinsic in natural landscapes, it is well suited for reconnaissance or regional landslide assessments. This investigation evaluates PISA-m as a regional landslide susceptibility modeling tool, specifically in the common use case of sparse geotechnical data, by computing eight susceptibility models using four soil input layers and parameter

Table 1. The eight models, four cases over two specifications, used to evaluate the practicality and utility of the PISA-m slope stability program for landslide susceptibility models.

[Abbreviations: KYTC, Kentucky Transportation Cabinet; USCS, Unified Soil Classification System; SSURGO, Natural Resources Conservation Service Soil Survey Geographic Database]

Model	Parameter specification	Soil input case	Assessment inventory
A1	A. Approximating background climatic conditions	1. Shale bed	Historic
A2		2. Geological formation	
A3		3. USCS (SSURGO)	
A4		4. Generalized USCS (SSURGO)	
B1	B. Approximating extreme rainfall event	1. Shale bed	Rapid reconnaissance
B2		2. Geological formation	
B3		3. USCS (SSURGO)	
B4		4. Generalized USCS (SSURGO)	

specifications approximating two climatic scenarios defined by landslide inventories within eastern Kentucky study areas. These eight models, with each of the four soil inputs applied to both parameter specifications, are outlined in Table 1. These models are defined by unique input soils map layers and associated geotechnical data. Geotechnical data were obtained from Kentucky Transportation Cabinet (KYTC) reports and related publications, with the exception of a generalized case using typical values for Unified Soil Classification System (USCS) classes for comparison.

The climatic scenarios assessed over the eight models were selected based on the availability of landslide inventories for model validation. Validation was done using the statewide historic inventory (Crawford, 2014, 2022), which represents typical landslide conditioning factors, and the July 2022 extreme rainfall inventory (Crawford et al., 2023), which represents extreme event-based conditions. Inventory landslides that occurred after the date of DEM data collection were intersected with the PISA-m results to estimate PISA-m performance. Using both inventories for validation allowed the performance of PISA-m to be assessed for both typical and extreme scenarios, or rather for both time-independent and event-specific scenarios.

Model Inputs

DEM

The DEM was derived from airborne lidar data and processed to a United States Geological Survey (USGS) Quality Level of 2 (Heidemann, 2012) with a spatial resolution of 1.5 m (5 ft). The DEM was resampled to ~3 m (10 ft) cell size for computing efficiency. Differences in preliminary results were not apparent when comparing models created from the 1.5 m DEM to models created from the 3 m DEM (Crawford et al., 2019). The DEM was "smoothed," a local averaging of elevation values using neighboring values within a moving circular window, to remove potential errors and holes in the DEM and reduce noise in the output PISA-m models. Window size was chosen through comparative testing of 7.5 m (25 ft) increments, and a radius of 15 m (50 ft) was found to best preserve the unsmoothed topographic characteristics of the DEM while minimizing noise and potential anomalies.

Forest Cover

The forest cover map input shows spatial distributions of forested areas to satisfy the tree surcharge and root strength components of the infinite slope equation. The National Land Cover Database (NLCD; Dewitz and U.S. Geological Survey, 2021) raster was reclassified using existing forest cover classes to serve as a binary raster of forested and bare areas. The NLCD raster was far coarser than the other inputs used and showed jagged edges even after resampling. An alternative forest cover extent raster was created by processing lidar point cloud data using a procedure similar to that described by Swallom et al. (2025). The DEM was subtracted from unclassified lidar returns to obtain vegetation height, which was further divided into forested and bare categories based on a 5 m (16.4 ft) threshold for trees (FGDC, 2008). Further processing was performed by smoothing the initial tree layer with a ~7.5 m (25 ft)

moving circular window (based on tree crown envelope diameters) to reduce noise in the forested areas. Comparison with aerial photography acquired in the same year as the lidar data showed consistency with the photographed canopy (Fig. 3).

Soil Layer Variation

Three soil map layers were used across the eight models: a map of shale beds, a bedrock formation map, and a soils map represented by USCS classes.

The shale bed layer (used for case 1) was modified from Chapella et al. (2019) and used the known influence of shale beds on landslide occurrence (Outerbridge, 1987; Crawford, 2014; Chapella et al., 2019). To spatially highlight shale beds, shale arc polylines were buffered to a ~30 m (100 ft) width and appended to a 1:24,000 bedrock lithology map in GIS. The geological units were combined into a single colluvium group, assuming near homogenous colluvial soil composition across the geological units. This was similar to the approach of Haneberg et al. (2009), who used surficial mapping to distinguish between areas of thick and thin colluvium in a project area in San Francisco.

The geological layer (used for case 2) used a 1:24,000 scale bedrock formation map as a proxy for soil type. This method assumed that bedrock formation spatial extents are useful predictors of the soil geotechnical parameters used in PISA-m and was similar to the bedrock-based approach taken by Stillwater Sciences (2007) and Weppner et al. (2008).

The soils map used broad Natural Resources Conservation Service Soil Survey Geographic Database (SSURGO; NRCS, 2023) spatial extents grouped into USCS soil units. The soil map layer is used for both case 3 and 4.

These layers, along with the DEM and binary forest cover raster maps, were clipped to the study areas and converted to ASCIIs for use in PISA-m. The DEM and forest cover layers were used for all eight models (Fig. 4).

Geotechnical Inputs

The geotechnical input parameters and values used were split into two groups based on climatic/rainfall scenarios. The typical background climatic conditions, approximated with geotechnical parameters in specification A (models A1–A4), were used to model landslide probabilities in static, non-seasonal conditions. Therefore, the geotechnical values used as PISA-m inputs needed to represent a full range of possible values throughout a year or many years. In order to assess the utility of PISA-m for modeling slope stability following an extreme rainfall event, models B1–B4 needed to account for the impact of the rainfall event by using more characteristic geotechnical values. This was done by modifying the distribution and value range of the

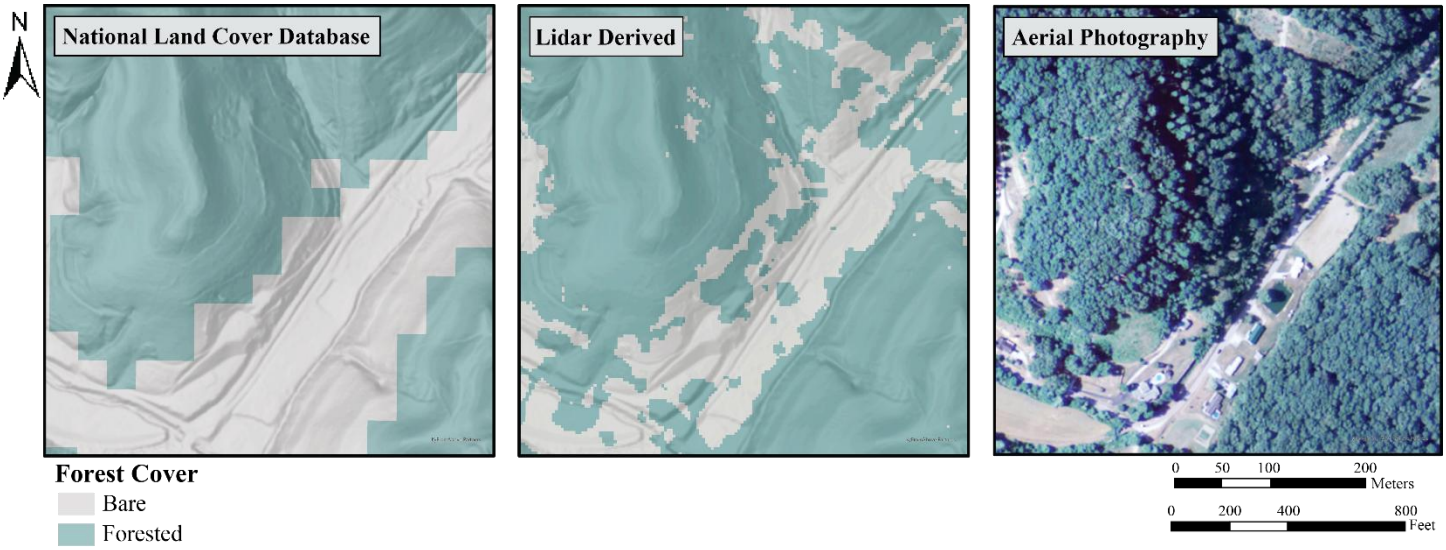

Figure 3. Comparison of the National Land Cover Database (Dewitz and U.S. Geological Survey, 2021) forest cover layer, the lidar-derived forest cover layer, and the canopy as seen from 2012 aerial photography (NAIP, 2012).

normalized height of the phreatic table (H_w) parameter to approximate full saturation of slopes during the extreme rainfall event. When these geotechnical values were not modified to account for the extreme rainfall event, preliminary model results underpredicted landslide occurrence when compared the extreme event inventory. Despite the phreatic table consideration and the order of magnitude difference in temporal scale, many of the other geotechnical values used were consistent between the cases and specifications due to data scarcity and the simplified nature of this study.

The geotechnical values used for cases 1–3 were modified from geotechnical boring information from KYTC and applicable studies (Sidle et al., 1985; Hammond et al., 1992; Haneberg, 2004; Chapella et al., 2019; Tables 2–4). The generalized soil case, 4, used easily accessible and generalized geotechnical examples for input data, such as those defined in textbooks (Anderson and Sitar, 1995; Budhu, 2007; Das, 2010; Table 5). Geotechnical values related to forest cover were gathered from similar studies that also used this version of the infinite slope equation (Hammond et al., 1999; Chapella et al., 2019; Table 6). Modifications made to these datasets included the reduction of internal friction angles (ϕ) and the zeroing of soil cohesion (c_s). These modifications have been used in similar analyses in the regional analogues of western Pennsylvania and Wheeling, West Virgina (Hamel, 1980; Haneberg, 2004), to represent residual shear strength characteristics instead of peak or typical shear strength. It is unclear if the geotechnical data sources used in this study report peak shear strength, so the reductions were performed as a precautionary measure.

As for distributions, a uniform distribution was used for a majority of the geotechnical variables due to limited information regarding the distribution shapes of the variables (Hammond et al., 1992). Two exceptions to the uniform distribution selection were tree surcharge, which used a normal distribution as prescribed by Chapella et al. (2019), and specification A phreatic table height, which used an extreme value type I distribution. Characterizing the phreatic table height (H_w) is particularly difficult due to variation caused by the

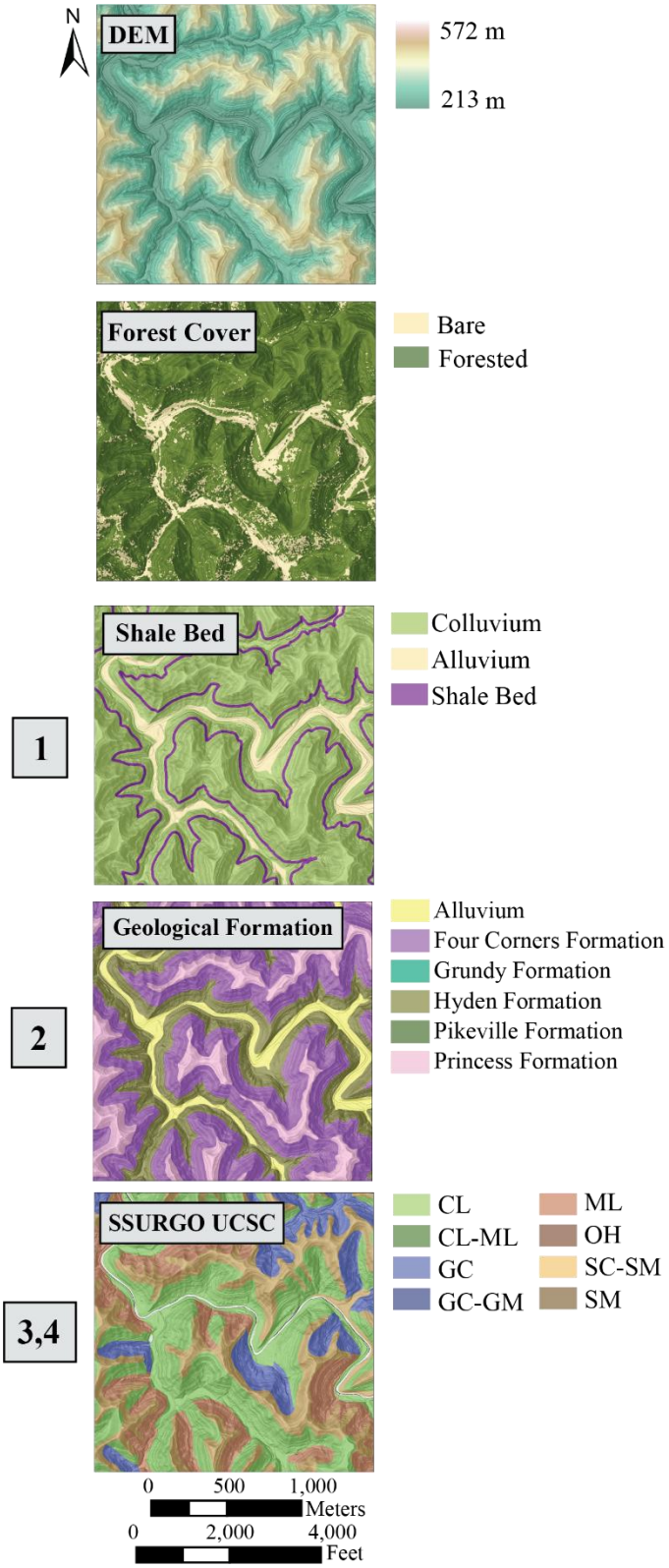

Figure 4. Inset examples of PISA-m input layers used for this study: the DEM, forest cover layer, and three soil map layers used in the eight models (shale bed, geological formation, and the UCSC soil classes). The numbers to the left of the soil layers correspond to model cases detailed in Table 1.

Table 2. Geotechnical values for the combined geological units (colluvium group), alluvium, and shale beds, modified from Kentucky Transportation Cabinet drilling report data and additional studies (Sidle et al., 1985; Hammond et al., 1992; Haneberg, 2004; Chapella et al., 2019).

Variable	Model	Distribution	Alluvium		Colluvium		Shale	
			Min.	Max.	Min.	Max.	Min.	Max.
Internal friction, ϕ (deg)	A1, B1	Uniform	17	33	22	33	17	24
Cohesion, c_s (Pa)	A1, B1	Uniform		0		0		0
Soil thickness, D (m)	A1, B1	Uniform	6.1	12.2	1.5	18.3	0.61	43.9
Pore pressure coefficient, from H_w (unitless)	A1	Extreme[1]	0.5	0.1	0.5	0.1	0.5	0.1
H_w (unitless)	B1	Uniform	0.75	1	0.75	1	0.75	1
Saturated unit weight, γ_{sat} (N/m^3)	A1, B1	Uniform	19,680.52	21,719.96	18,252.92	22,943.61	21,210.10	23,147.56
Moist unit weight, γ_m (N/m^3)	A1, B1	Uniform	19,068.69	22,369.16	15,091.80	24,065.30	20,904.18	26,614.59

[1]Extreme (Gumbel) distribution uses location and shape parameters instead of the minimum and maximum values used by the uniform distribution.

Table 3. Geotechnical values for bedrock formations, modified from Kentucky Transportation Cabinet drilling report data and additional studies (Sidle et al., 1985; Hammond et al., 1992; Haneberg, 2004; Chapella et al., 2019).

Variable	Model	Distribution	Alluvium		Four Corners		Grundy, Hyden, and Pikeville		Princess	
			Min.	Max.	Min.	Max.	Min.	Max.	Min.	Max.
Internal friction, ϕ (deg)	A1, B1	Uniform	17	33	17	24	17	24	15	27
Cohesion, c_s (Pa)	A1, B1	Uniform		0		0		0		0
Soil thickness, D (m)	A1, B1	Uniform	0.3	0.91	0.61	3.05	0.61	43.9	0.3	0.91
Pore pressure coefficient, from H_w (unitless)	A1	Extreme[1]	0.5	0.1	0.5	0.1	0.5	0.1	0.5	0.1
H_w (unitless)	B1	Uniform	0.75	1	0.75	1	0.75	1	0.75	1
Saturated unit weight, γ_{sat} (N/m^3)	A1, B1	Uniform	18,850.50	20,892.64	20,421.38	22,306.43	17,436.71	21,992.25	17,436.71	21,992.25
Moist unit weight, γ_m (N/m^3)	A1, B1	Uniform	17,907.98	22,306.43	20,107.20	25,605.26	14,452.05	23,091.86	14,452.05	23,091.86

[1]Extreme distribution uses location and shape parameters instead of the minimum and maximum values used by the uniform distribution.

Table 4. Geotechnical values for United Soil Classification System units, modified from Kentucky Transportation Cabinet drilling report data and additional studies (Sidle et al., 1985; Hammond et al., 1992; Haneberg, 2004; Chapella et al., 2019).

Variable	Model	Distribution	CL, Cl-ML		CG, GC-GM		ML, OH		SC-SM		SM	
			Min.	Max.	Min.	Max.	Min.	Max.	Min.	Max.	Min.	Max.
Internal friction, ϕ (deg)	A1, B1	Uniform	24	32	24	33	23	33	24	31	23	33
Cohesion, c_s (Pa)	A1, B1	Uniform		0		0		0		0		0
Soil thickness, D (m)	A1, B1	Uniform	1.5	18	1.5	18	6	12	1	6	6	12
Pore pressure coefficient, from H_w (unitless)	A1	Extreme[1]	0.5	0.1	0.5	0.1	0.5	0.1	0.5	0.1	0.5	0.1
H_w (unitless)	B1	Uniform	0.75	1	0.75	1	0.75	1	0.75	1	0.75	1
Saturated unit weight, γ_{sat} (N/m^3)	A1, B1	Uniform	17,986.81	19,997.56	19,997.56	21,992.60	15,991.76	21,992.60	17,986.81	19,997.56	17,986.81	19,997.56
Moist unit weight, γ_m (N/m^3)	A1, B1	Uniform	13,981.01	17,908.26	14,986.39	16,965.72	13,981.01	20,892.97	12,991.34	15,991.76	12,991.34	15,991.76

[1]Extreme distribution uses location and shape parameters instead of the minimum and maximum values used by the uniform distribution.

Table 5. Geotechnical values for United Soil Classification System units, derived from a data repository hosted by www.geotechdata.info and other accessible, generalized data (Anderson and Sitar, 1995; Budhu, 2007; Das, 2010).

Variable	Model	Distribution	CL, Cl-ML		CG		GC-CM		ML		OH		SC-SM		SM	
			Min.	Max.	Min.	Max.	Min.	Max.	Min.	Max.	Min.	Max.	Min.	Max.	Min.	Max.
Internal friction, ϕ (deg)	A1, B1	Uniform	24	32	25	32	27	37	24	32	22	32	27	37	24	30
Cohesion, c_s (Pa)	A1, B1	Uniform		0		0		0		0		0		0		0
Soil thickness, D (m)	A1, B1	Uniform	1.5	18	1.5	18	1.5	18	6	12	6	12	1	6	6	12
Pore pressure coefficient, from H_w (unitless)	A1	Extreme[1]	0.5	0.1	0.5	0.1	0.5	0.1	0.5	0.1	0.5	0.1	0.5	0.1	0.5	0.1
H_w (unitless)	B1	Uniform	0.75	1	0.75	1	0.75	1	0.75	1	0.75	1	0.75	1	0.75	1
Saturated unit weight, γ_{sat} (N/m^3)	A1, B1	Uniform	14,000.00	18,000.00	20,000.00	22,000.00	20,000.00	22,000.00	16,000.00	22,000.00	16,000.00	22,000.00	18,000.00	20,000.00	18,000.00	20,000.00
Moist unit weight, γ_m (N/m^3)	A1, B1	Uniform	18,000.00	20,000.00	15,000.00	17,000.00	15,000.00	17,000.00	14,000.00	21,000.00	14,000.00	21,000.00	13,000.00	16,000.00	13,000.00	16,000.00

[1]Extreme distribution uses location and shape parameters instead of the minimum and maximum values used by the uniform distribution.

Table 6. Geotechnical values for tree surcharge and root cohesions, modified from Chapella et al. (2019). Bare cover was considered as a constant of zero.

Variable	Distribution	Min.	Max.	Mean	Standard deviation
Root cohesion, *cr* (Pa)	Uniform	5,700	6,900	—	—
Tree surcharge, *qt* (Pa)	Normal	—	—	2,500	±500

frequency and duration of rainfall events as well as antecedent moisture conditions (Haneberg, 2000). Haneberg (2000) describes the significant impact of normalized phreatic table height (H_w), and the related pore pressure coefficient, on changes to factor of safety. To accurately account for the pore pressure coefficient, the extreme value type I distribution was used to approximate annual variation (Weppner et al., 2008) for the analyses in models A1–A4. Models B1–B4 instead had geotechnical values and distributions selected with the rainfall duration and frequency data recorded over a four-day extreme rainfall event (Crawford et al., 2023) in mind. In general, soil moisture conditions before and during rainfall events are not well known or characterized. Haneberg and Gökce (1994) considered soil moisture characteristics observed from a landslide deposit in colluvial slopes near Cincinnati, Ohio, and found that soil moisture responded rapidly to rainfall events. Considering the relatively dry summer season experienced in eastern Kentucky in July 2022 and the magnitude of the extreme rainfall event (NWS, 2023), lag effects may not be applicable, and a similarly rapid rise in phreatic table height may be assumed for this event. As such, values for H_w with a uniform distribution were selected in specification B (models B1–B4) to represent near or fully saturated conditions.

Model Assessment Method

To quantify the performance of the PISA-m models, buffered landslide points were intersected with the results. These points represented historic landslides that occurred after DEM creation in locations 1 and 2 (~2012 for areas within Perry County and Magoffin County, ~2017 for other areas) and the landslides identified from rapid reconnaissance following a July 2022 extreme rainfall event (Crawford et al., 2023). A total of 37 historic landslides (16 in location 1 and 21 in location 2) with failure dates between 2011 and 2022 were used to represent the background climatic scenario and assess models A1–A4. For models B1–B4, which used parameter specifications to approximate the extreme rainfall scenario, 1,068 landslides from the rapid reconnaissance inventory were used to assess model performance. The observed landslides in the rapid reconnaissance inventory correspond to a small date range (July 14–18, 2022). The extreme rainfall scenario (and related specification B) is defined by an anomalous four-day rainfall total of 360–410 mm (14–16 in.). In comparison, over the decade considered in the background climatic conditions scenario (and specification A), average total annual rainfall was 130 mm for location 1 and 110 mm for location 2 (PRISM, 2024). The historic inventory landslides with recorded dates largely occurred within late winter and early spring. Figure 5 compares rainfall to historic landslide occurrences.

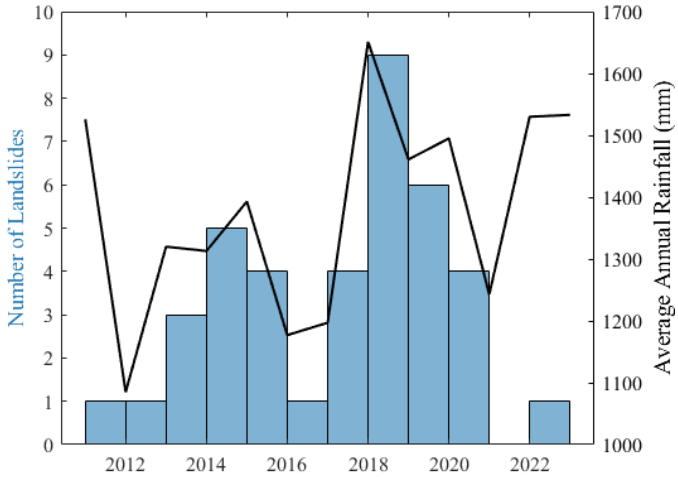

Figure 5. Histogram of landslide counts (blue bars) from the historic inventory in the study area compared to average rainfall data from PRISM (black line).

To approximate a landslide deposit and to cover potential initiation zones, an arbitrary ~15 m (50 ft) buffer was assigned to each point and intersected with the PISA-m model results. This arbitrary buffer was used for ease of reproducibility in situations of information scarcity. In most instances, 15 m may be an underestimation of landslide initiation zone sizes. However, this smaller size constraint on the inventory buffers used for PISA-m assessment was preferred over capturing distant high Prob[$FS \leq 1$] values that were disconnected

from the landslide in question. The buffered landslide points were used to gather the mean and maximum Prob[$FS \leq 1$] value from each landslide area. Higher mean probability values (i.e., Prob[$FS \leq 1$] > 0.50) for known slope failure areas were considered accurate model characterization (Haneberg, 2004; Chapella et al., 2019). Accurate prediction/success rates were determined by assessing the number of landslides in each inventory that intersected with Prob[$FS \leq 1$] > 0.50 areas.

Further, the models were checked for overfitting, which could result in the model predicting high susceptibility across the entire landscape. To perform an overfitting assessment, an equal number of negative samples, or non-landslide points, are needed to balance the landslide points. As such, to assess models A1–A4, 37 non-landslide points were needed to balance the historic inventory, and to assess models B1–B4, 1,068 non-landslide points were needed balance the rapid reconnaissance inventory. These non-landslide points were also buffered 15 m and intersected with model results. Although using an equal number of positive and negative samples avoids bias towards the larger class (Blagus and Lusa, 2010), landslide assessment would imply a much larger area of non-landslide activity. To constrain non-landslide point selection to be more representative of these stable environments, GIS-based controls were applied. First, buffers of ~60 m (200 ft) were generated around landslide points from both the historic and rapid reconnaissance inventories and around digitized landslide deposit extents in location 2 only (Crawford et al., 2021, 2023). Digitized landslide extents were not available in location 1 during this study. These buffered landslide areas were omitted from non-landslide point selection areas. Second, mean slope angles from each landslide inventory were determined and used as approximate thresholds for slopes more primed for failure. As such, areas above 24.3° for location 1 and 28.9° for location 2 were omitted from the non-landslide selection area. This slope angle thresholding was done to ensure that existing but unconfirmed or unmapped landslides were not considered in model assessment. Third, to minimize the effects of the random generation, such as non-landslide points clustering in similar topographic areas, five distinct non-landslide point datasets were randomly generated for each location. Each of these five non-landslide point datasets was intersected with model results, and those five sets of intersections were averaged to produce the single non-landslide dataset needed for Prob[$FS \leq 1$] comparisons. This averaging of non-landslide datasets worked as a form of cross validation.

To consider potential bias of the roadway-based reconnaissance efforts that created the extreme event inventory, the rapid reconnaissance inventory was intersected with a Euclidean distance-to-roads raster. This showed an average distance from slides to roadways of 54 m (177 ft), with a maximum distance of ~1,130 m (3,700 ft). Noting these distances, non-landslide points were generated within 61 m (200 ft; mean distance from road plus radius of landslide area) and 305 m (1,000 ft) of roads in the study area, with slope angle thresholds and landslide areas considered. These landslide and non-landslide area intersections with the PISA-m results were assessed using confusion matrices. True positives (*TP*) were determined from intersections of Prob[$FS \leq 1$] > 0.50 with landslide areas, and where landslide areas intersected with Prob[$FS \leq 1$] < 0.50, they were classed as false negatives (*FN*). Model results of Prob[$FS \leq 1$] > 0.50 that intersected known non-landslide areas were considered false positives (*FP*), and results with Prob[$FS \leq 1$] < 0.50 in non-landslide areas were classed as true negatives (*TN*). Model performance is defined by confusion matrix accuracy (*ACC*), which is calculated as

$$ACC = \frac{TP + TN}{TP + FP + TN + FN}, \tag{4}$$

where accuracy is derived from the relationship between the sum of *TP* and *TN* divided by the sum of all classifications (Ting, 2017; Chicco and Jurman, 2020).

Chicco and Jurman (2020) proposed the adoption of the Matthews correlation coefficient (*MCC*). *MCC* uses an approximate calculation of the Pearson product-moment correlation coefficient (Powers, 2011). *MCC* is defined by

$$MCC = \frac{TP \times TN - FP \times FN}{\sqrt{TP + FP \times TP + FN \times TN + FP \times TN + FN}} \tag{5}$$

and is normalized with

$$nMCC = \frac{MCC + 1}{2}. \quad (6)$$

Normalized *MCC* was assessed as a check for other metrics. The *MCC* metric focuses on correct predictions, *TP* and *TN*, and returns a favorable score when those cases are a majority of the assessment. *MCC* is best utilized on unbalanced datasets, but the focus on *TP* and *TN* majority is useful even for intentionally balanced cases such as this assessment.

Results

Results for each of the eight models were computed for Prob[$FS \leq 1$] under static (non-seismic) conditions and imported into GIS for further analysis. The resulting Prob[$FS \leq 1$] raster maps were symbolized as five groups based on equal intervals, following Kentucky Geological Survey (KGS) conventions (Crawford et al., 2021). Slope angles below 5° were automatically omitted from the model results.

Specification A
Background Climatic Scenario

PISA-m results were similar for each of the specification A models, highlighting planar slope faces and subtle cliff and bench topography with Prob[$FS \leq 1$] of 0.50 or higher. For the shale bed cases and both USCS cases, the smooth planar slopes, as well as where the slopes transition into hollows, were uniformly classified with Prob[$FS \leq 1$] > 0.50. In the geological formation case, these same areas of planar slope faces and hollow transitions had a wider range of Prob[$FS \leq 1$] values present. The geological formation case also had a more pronounced influence from the forest cover layer, especially where low slope angle areas near ridgetops had gaps in the canopy. These holes in forest cover were represented in PISA-m model results by stark concentrations of high Prob[$FS \leq 1$] > 0.50. In general, areas of lower slope angles had Prob[$FS \leq 1$] < 0.50. Prob[$FS \leq 1$] > 0.50 values were dominant in areas where incision was sharper and slope angles increased. Differences between the two USCS cases were very small, with the generalized case having overall lower Prob[$FS \leq 1$] values in some areas (particularly broad hollows). The shale bed case was the only model resulting in higher Prob[$FS \leq 1$] values near the ridgetops. Inset examples for specification A model results are seen in Figure 6 and Figure 7.

Specification B
Extreme Rainfall Scenario

The specification B models characteristically had a significant coverage of high Prob[$FS \leq 1$] values across the landscape. PISA-m models with this specification attempted to account for the extreme rainfall event precipitation and subsequent increase in landslide occurrence by adjusting the model inputs and as a result, a majority of the landscape was considered susceptible to landslide occurrence. That is, PISA-m calculated Prob[$FS \leq 1$] > 0.50 for nearly all slopes above 22°. The geological formation case had a wider range of Prob[$FS \leq 1$] values represented, preserving wide benches in the hillsides as areas where Prob[$FS \leq 1$] < 0.50. The shale bed case and both USCS cases output Prob[$FS \leq 1$] > 0.50 for a majority of the slopes. These cases were largely indistinguishable from one another, with a slight reduction in the overall Prob[$FS \leq 1$] values in the generalized USCS case (B4) and report-derived USCS case (B3). Shale bed and USCS results extended Prob[$FS \leq 1$] > 0.50 to the ridgetops, whereas the geological formation case (B2) indicated lower Prob[$FS \leq 1$] values near ridgetops, these value reductions matching the mapped extent of a sandstone unit. Similar to the results for specification A, these formation-controlled areas with low Prob[$FS \leq 1$], as well as other low slope angle areas, show that clearings in the forest cover raster influence model results. Inset examples of the model results for specification B can be seen in Figure 7. Area coverage percentages for each susceptibility group are shown in Table 7.

Model Assessment Results

Model results were intersected with landslide and non-landslide areas. Success rates (only considering *TP*) for each model are shown in Table 8.

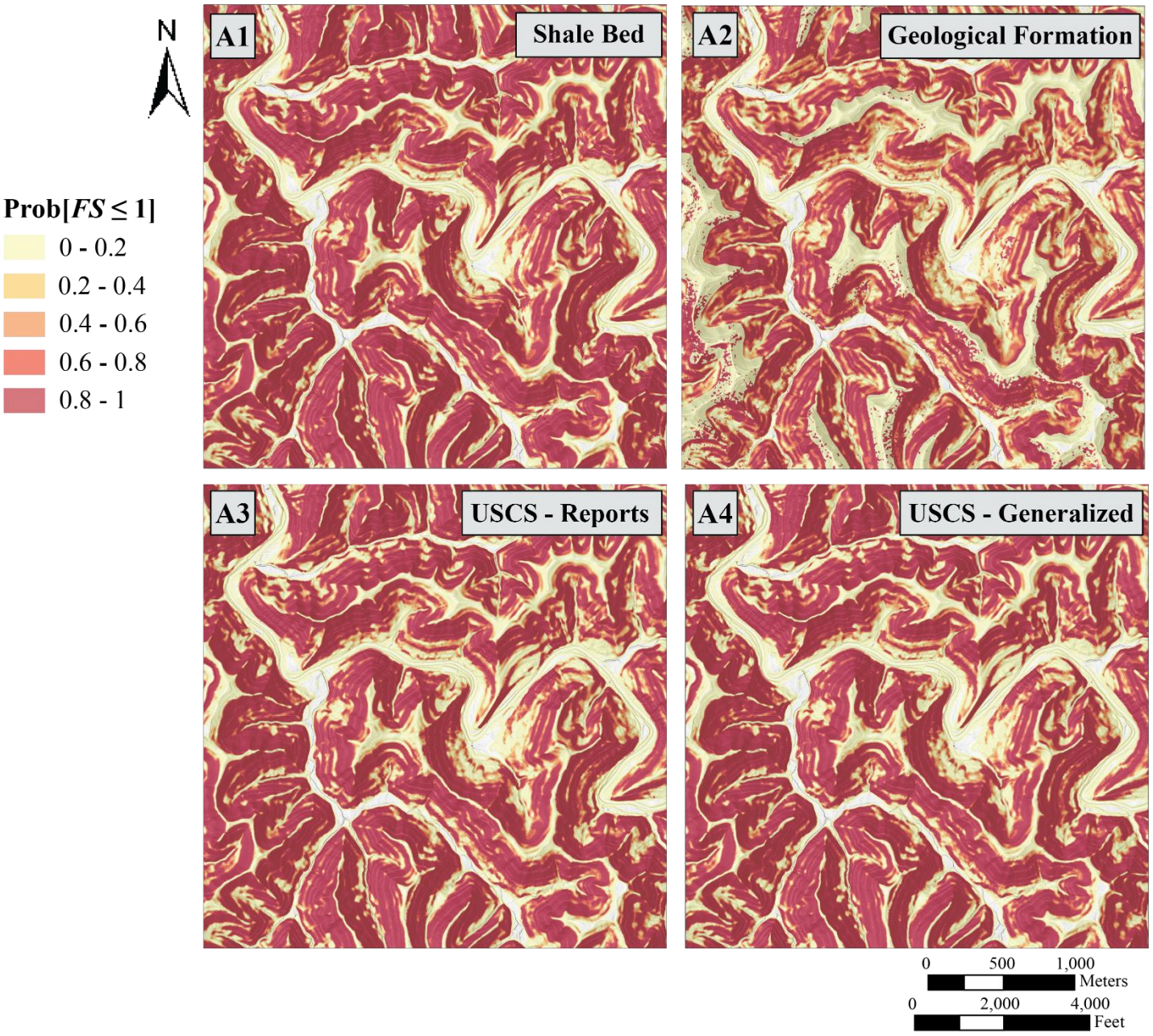

Figure 6. Inset PISA-m results for the four cases using the parameters in specification A, which approximates a background climatic conditions scenario. Models numbered and labeled per Table 1.

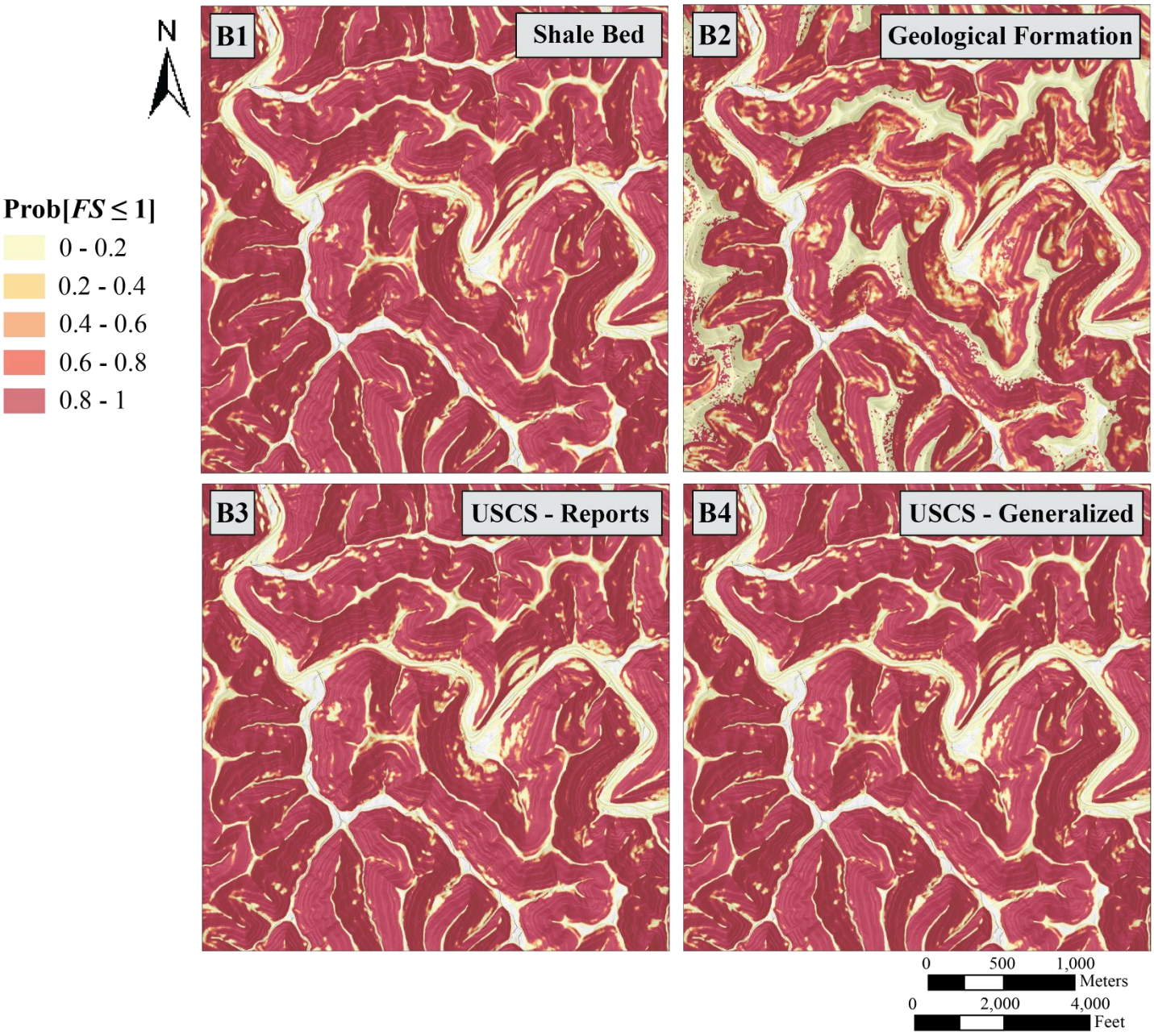

Figure 7. Inset PISA-m results for the four cases using the parameters in specification B, which approximates an extreme rainfall event scenario. Models numbered and labeled per Table 1.

Table 7. Percent area coverages of the Prob[$FS \leq 1$] model results divided into five equal interval groups for each model.

Model	Prob[$FS \leq 1$]				
	0–0.2	0.2–0.4	0.4–0.6	0.6–0.8	0.8–1.0
A1	28.6%	6.8%	6.9%	9.0%	48.6%
A2	36.7%	8.6%	9.0%	12.3%	33.5%
A3	31.1%	6.9%	6.9%	9.0%	46.2%
A4	31.7%	6.4%	6.4%	8.2%	47.3%
B1	17.0%	4.0%	4.3%	6.0%	68.8%
B2	24.7%	6.4%	7.1%	10.8%	51.0%
B3	17.2%	3.7%	3.9%	5.5%	69.8%
B4	17.7%	3.3%	3.4%	4.7%	70.8%

Table 8. Success rates of each model with the respective landslide inventory.

Inventory	Model	Success rate (%)
Historic	A1	75.7
	A2	75.7
	A3	78.4
	A4	78.4
Rapid reconnaissance	B1	83.5
	B2	75.7
	B3	82.5
	B4	81.9

Further assessment included non-landslide points along with the landslide points to calculate metrics based on confusion matrix relationships. The historic inventory points for both location 1 and 2 were used for the specification A models, or those approximating a background climatic scenario, and when paired with the averaged non-landslide dataset yielded confusion matrix derived model accuracies of 72.97%, 82.43%, 79.73%, and 77.03% for the shale bed, geological formation, report-derived USCS, and generalized USCS cases, respectively. To assess specification B models, or those approximating the extreme rainfall scenario, a two-tailed Student's t-test (Kalpić et al., 2011) was used to test for similarity in the non-landslide points concentrated around roadways. Non-landslide points within 300 m of roads did not have statistically distinguishable mean Prob[$FS \leq 1$] values from those of non-landslide points generated more than 300 m from the roadway ($p > 0.05$). However, points generated within 61 m of roads were statistically distinct from points from across the study area ($p < 0.05$). Since the rapid reconnaissance inventory points were on average 54 m from the roadway, the roadway-constrained non-landslide points were considered more suitable for comparison to the rapid reconnaissance inventory. Additionally, model accuracies improved by about 5% when using the roadway-constrained negative samples. The rapid reconnaissance inventory, when compared to an averaged, roadway-constrained, non-landslide dataset, showed model accuracies of 84.04%, 83.90%, 83.52%, and 83.33% for the shale bed, geological formation, report-derived USCS, and generalized USCS cases, respectively. The additional assessment metrics beyond confusion matrix accuracy indicate stable model results (Table 9). Confusion matrix assessments for both specifications are seen in Figures 8 and 9.

Table 9. Performance metrics across all models. In general, model performance was consistent across metrics.

Model	Accuracy (%)	Matthews Correlation Coefficient, normalized (*nMCC*)
A1	72.97	0.73
A2	82.43	0.83
A3	79.73	0.8
A4	77.03	0.77
B1	84.04	0.84
B2	83.90	0.84
B3	83.52	0.84
B4	83.33	0.83

Discussion

Using PISA-m to model an extreme scenario (specification B) appears to be the better utilization of the modeling program based on higher confusion matrix assessment accuracies, but those high Prob[$FS \leq 1$] values could be overpredictions, as many slope faces have Prob[$FS \leq 1$] > 0.50. However, the variability of the shale bed case, a high-performing model by accuracy when using specification B yet the lowest overall when using specification A, may just be the byproduct of the larger sample size. Overall, the highest false positive rate was 12% (models A1, A2, and B2), and the lowest was 8 to 9% (models B1 and B3), indicating that the models rarely misclassed non-landslides.

Point landslide observations may not be indicative of all possible landslide failure characteristics, thus increasing the false positive rate, as any model's focus on a

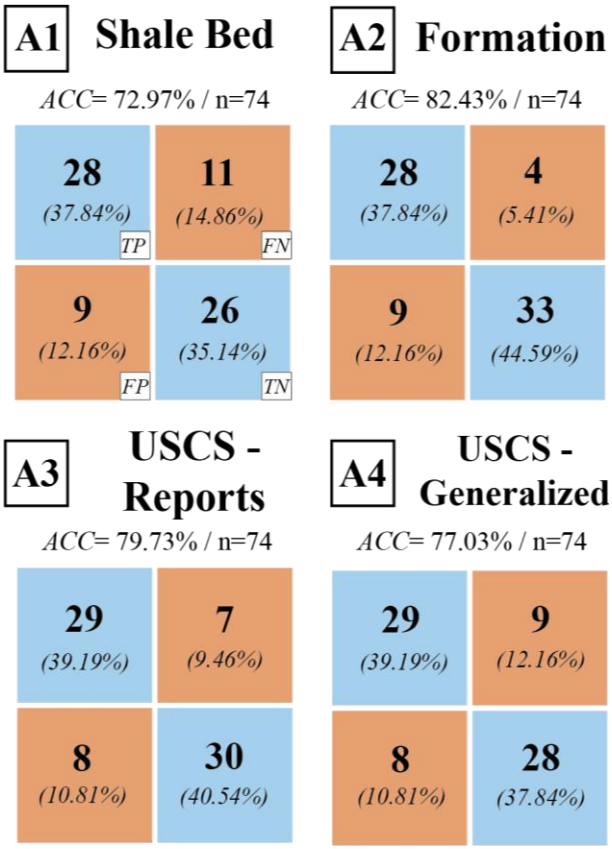

Figure 8. Confusion matrices for the PISA-m results for each of the four cases using specification A. Models numbered per Table 1. Note true positive (*TP*), true negatives (*TN*), false positives (*FP*), and false negatives (*FN*) labels in A1.

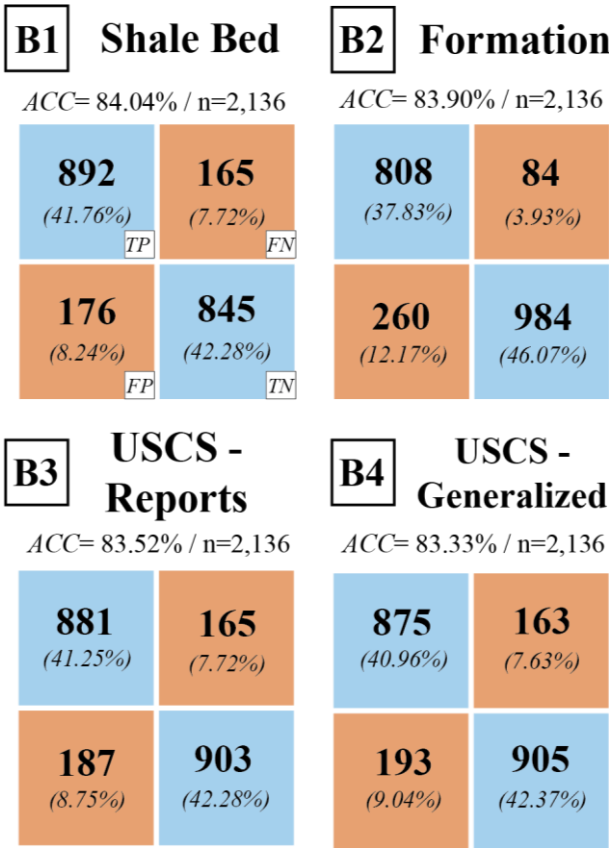

Figure 9. Confusion matrices for each of the four PISA-m cases using specification B. Models numbered per Table 1. Note true positive (*TP*), true negatives (*TN*), false positives (*FP*), and false negatives (*FN*) labels in B1.

specific landslide failure type may cause overprediction regionally. This may have occurred with the rapid reconnaissance inventory, as the points were mostly close to roadways, and model assessments were improved when non-landslide points were generated with roadway proximity in mind. These improvements in the model performances may also be due to the other constraints, such as forcing non-landslide points off hillslopes. While constraining the non-landslide points improved the metrics, potential overprediction of Prob[$FS \leq 1$] on slopes may have been overlooked. The buffers applied to points to create initiation zones or represent deposits could also lead to uncertainty in model performance. However, a conservative size was chosen to reduce this effect. Swallom et al. (2025) found a 16.7 m buffer appropriate to approximate landslide areas with the same extreme rainfall inventory. In general, comparison to any available landslide extent data should be able to inform the selection of an appropriate buffer size for landslide inventory points. Non-landslide point selection is a particular area of focus in contemporary landslide susceptibility modeling (Hu et al., 2020; Khabiri et al., 2023; Zhou et al., 2024) because constrained non-landslide point selection has been proven to yield higher performing models. For example, Khabiri et al. (2023) used low Prob[$FS \leq 1$] results from PISA-m, with a version of the shale bed case, as a control for non-landslide point selection. Zhou et al. (2024) deployed a similar approach, instead using a logistic regression model output to select the non-landslide points. For simplicity, only the GIS-based constraints discussed previously were used for this study. Even when constrained by slope angle and known landslide locations, the assumption persists that randomly selected non-landslide points do not intersect a landslide. Slope angle thresholding may assist in reducing these overlaps, as the hypothetical non-identified landslide would be atypical of other slides in the inventory. The omission of areas around the digitized landslide polygon inventory (Crawford et al., 2021) of location 2

increased confidence that landslides were not inadvertently included in the non-landslide case. Further, by averaging five sets randomly sampled non-landslide point datasets, the influence of spurious points was reduced. The rapid reconnaissance inventory lacks confidence in landslide locations, and with some of the landslide points plotted within the floodplain or on the road (likely where the landslide deposit reached), the landslide point locations may be inexact. Swallom et al. (2025) noted that overall, the rapid reconnaissance inventory points fit into general geomorphic landform classes, or geomorphons, (Jasiewicz and Stepiski, 2013) representing typical hillslope areas, inferring a lack of bias of points along roadways. Despite this, the t-test indicated that points generated in close proximity to roads had statistically distinct Prob[$FS \leq 1$] values, so only non-landslide points generated near roadways were used. These roadway-constrained points increased assessment accuracies, primarily by decreasing *FP*. Again, this is likely due to the concentration of points in low value Prob[$FS \leq 1$] areas. In general, applying constraints to the landslide inventories improved the assessments. At worst, when considering a randomly sampled non-landslide point set (with the only constraint being the omission of known landslide extents), the model performance was about 30% lower. Regardless, it is unclear how these constrained points may have artificially inflated model performance, as potential overprediction on high slope angles was not considered.

While meant to assess model performance, consideration of the inventory point intersections may have skewed some of the model interpretations. Ultimately, the assessments are a first-order test of over- or underprediction for the PISA-m models. If all known landslide points were missed (low *TP*), or conversely, if a majority of the determined non-landslide points were classed as unstable (low *TN*), then these PISA-m results could be rejected as having limited utility. Metrics that focus on the known landslide points (such as success rates; Table 8) were similar to accuracy, as were more robust metrics such as the *nMCC*. While an approximation, the favorable results from the point assessments are a good indicator that PISA-m works as a first-order investigation into regional landslide susceptibility. More thorough assessments using complete inventories are recommended, as are more thorough assessments of the geotechnical inputs themselves. It is difficult to discern the completeness of the historic point inventory used as a proxy for landsides occurring in background climatic conditions. This assumes that the 37 landslides that have occurred between 2011 and 2021 in the study areas are indicative of natural landslide occurrence rates, but there is little evidence to support this assumption. Preliminary work by the authors to generate difference maps between two series lidar datasets covering a similar date range have not yielded useful results due to quality level and spatial misalignment. As such, further investigation of landslide reoccurrence rates from lidar differencing is beyond the scope of this study. In lieu of differenced topography, constrained non-landslide point selection is ultimately necessary, especially with the uncertain distribution and frequency of landslide events. While the rapid reconnaissance inventory has a large sample size to draw conclusions from, inventories reflecting extreme conditions are not applicable to assessments of model results based on background climatic conditions. Instead, PISA-m should be used in a way that accounts for extreme scenarios. While an effort was made to account for the extreme conditions, using the program configuration assessed in this study (an intentionally "off-the-shelf" variety), PISA-m is likely not well equipped to model this type of event. Further alterations to the pore pressure values and statistical distribution are needed to approximate extreme events of this magnitude. If using PISA-m for extreme event modeling, more specific calibration to an extreme event inventory would be useful. PISA-m, even when approximating different scenarios with parameter specifications, is still time independent. For instance, using recorded peak pore pressure distributions approaches a temporal model, but the specific ranges of geotechnical values needed to precisely model a given time period are unlikely to be obtained. Matching the time-independent probability results of PISA-m to failure rates and vice-versa can be more confusing than clarifying for end users (Haneberg, 2015).

Visual inspection of the model results shows consistency between the shale bed case and both USCS

cases across both specifications. Either the distinct methods of soil classification yield similar (and ultimately real) landscape-controlled landslide susceptibility, or the geotechnical values used in each case do not differentiate the soil inputs from one another. There are several geotechnical value similarities across the models, and despite the spatial distributions being vastly different between the shale bed case and the USCS cases, model results appear very similar. These similarities may not be an indication of poor model performance, however. Since these maps attempt to represent the same in-situ value ranges for soils and other slope characteristics, using similar values across the whole of the landscape is likely the more practical approach. If the values provided are extreme or an uncharacteristic distribution is applied, the results could include false positives. As a result, PISA-m appears less sensitive to the spatial extents of the input soils layer and more sensitive to the geotechnical values and probabilities assigned.

The widespread use of uniform distributions also contributes to a lack of confidence in the Prob[$FS \leq 1$], but the assumption of uniform distributions is necessitated by a lack of detailed geotechnical data available (Haneberg, 2004). Parker et al. (2016) argued that uniform distributions were valid in the southern Appalachians for saturated unit weights (γ_{sat}), internal friction angles (ϕ), and soil cohesions (c_s) but that uniform distributions poorly fit root cohesion (c_r) and soil thicknesses (D). Sidle and Wu (1999) found that soil cohesion and internal friction angles could be assumed to be uniformly distributed over their simulations. Root cohesion and morphology are noted as contributing more substantially to the factor of safety equation (Simons et al., 1978; Hammond et al., 1992). Additionally, as discussed, the height of the phreatic table (H_w) has a significant impact on model results. While uniformity can be assumed comfortably for some parameters, robust characterization of key parameters such as root cohesion and phreatic table height is advisable. Especially in the case of scarce data availability, well-defined geotechnical values and data distributions are essential for effective PISA-m utilization. While there were significant estimations made to assign geotechnical values, the spatial coverages of the soil units and the lidar-derived map-based inputs were more certain. Specifically, the use of high-resolution lidar derivatives to generate the forest cover spatial input, as well as further processing of the lidar-derived DEM, likely added to PISA-m's utility.

Conclusions

Eight distinct slope stability models, four cases across two parameter specifications, were applied to PISA-m and were assessed using two different inventories. The focus of this study was to assess the flexibility of inputs, the impact of sparse and uncertain geotechnical data, and ultimately, the practicality of PISA-m for use in regional landslide susceptibility modeling. By utilizing high-resolution lidar inputs when possible and prudently characterizing the geotechnical parameters, gaps and uncertainties within available data can be accounted for, and regional landslide susceptibility assessments can be generated efficiently. While this study did not assess the full range of possibilities, the easy-to-implement probability functionality of PISA-m separates the program from other physics-based models. The flexibility of the model inputs, the translatable factor of safety output, the limited computing power required, and the shorter analysis time are all benefits of using PISA-m. While this study assessed the sparse data use case, proper geotechnical assessments should still be conducted, if possible, to reduce significant sources of error in the model. Specific attention should be placed on deriving comprehensive data distributions and value ranges for key parameters such as height of phreatic table (H_w), root cohesion (c_r) and soil/colluvial thickness (D). While specific (extreme) scenario testing was performed through parameter specification and showed good merits when assessed, off-the-shelf PISA-m settings and approximate, time-independent geotechnical values should be used with caution. Despite these disclaimers, with good understanding of the study area and justifiable approximations of the physical characteristics of the soils, PISA-m can use available data to quickly generate regional susceptibility maps that serve as first-order assessments.

Acknowledgments

Initial research was supported by the Federal Emergency Management Agency Pre-Disaster Mitigation grant, project number PDMC-PL04-KY-2017-00, titled "Landslide Assessment and Mitigation Plan for the Big Sandy Area Development District." Lidar DEM and other essential base layer data were sourced from the Kentucky Division of Geographic Information (DGI) Kentucky from Above Program, the United States Department of Agriculture (USDA) provided SSURGO soils data. Thank you to Rachel Noble-Varney for encouragement, Dr. Zhenming Wang for feedback, and KGS researchers Dr. Junfeng Zhu and Doug Curl for thoughtful review. Thank you to KGS editor Shelby Fulton thorough editing and review. Thank you to Dr. Yichuan Zhu for optimizations to the PISA-m program. Thank you to Keiko Suzuki for feedback and support.

References Cited

Anderson, S.A., and Sitar, N., 1995, Shear strength and slope stability in a shallow clayey soil regolith, *in* Haneberg, W.C., and Anderson, S.A., eds., Clay and shale slope instability: Boulder, CO, Geological Society of America, Reviews in Engineering Geology 10, p. 1–11, https://doi.org/10.1130/REG10-p1.

Baum, R.L., Savage, W.Z., and Godt, J.W., 2008, TRIGRS—A Fortran program for transient rainfall infiltration and grid-based regional slope-stability analysis [ver. 2.0, 2009-10]: U.S. Geological Survey, Open-File Report 2008-1159, 75 p., https://doi.org/10.3133/ofr20081159.

Blagus, R., and Lusa, L., 2010, Class prediction for high-dimensional class-imbalanced data: BMC Bioinformatics, v. 11, article 523, https://doi.org/10.1186/1471-2105-11-523.

Budhu, M., 2011, Soil mechanics and foundations [3rd ed.]: Hoboken, NJ, Wiley, 761 p.

Capparelli, G., and Versace, P., 2011, FLaIR and SUSHI: Two mathematical models for early warning of landslides induced by rainfall: Landslides, v. 8, p. 67–79, https://doi.org/10.1007/s10346-010-0228-6.

Chapella, H., Haneberg, W., Crawford, M., and Shakoor, A., 2019, Landslide inventory and susceptibility models, Prestonsburg 7.5-min quadrangle, Kentucky, USA, *in* Shakoor, A., and Cato, K., eds., IAEG/AEG Annual Meeting proceedings, San Francisco, California, 2018: Cham, Switzerland, Springer, v. 1, p. 217–226, https://doi.org/10.1007/978-3-319-93124-1_26.

Chicco, D., and Jurman, G., 2020, The advantages of the Matthews correlation coefficient (MCC) over F1 score and accuracy in binary classification evaluation: BMC Genomics, v. 21, article 6, https://doi.org/10.1186/s12864-019-6413-7.

Crawford, M.M., 2014, Kentucky Geological Survey landslide inventory: From design to application: Kentucky Geological Survey, ser. 12, Information Circular 31, 18 p., https://doi.org/10.13023/kgs.ic31.12.

Crawford, M.M., 2022, Kentucky Geological Survey landslide inventory [ver. 3, 2023-03]: Kentucky Geological Survey, ser. 13, research data, https://doi.org/10.13023/kgs.data.2022.01.

Crawford, M.M., Dortch, J.M., Koch, H.J., Killen, A.A., Zhu, J., Zhu, Y., Bryson, L.S., and Haneberg, W.C., 2021, Using landslide-inventory mapping for a combined bagged-trees and logistic-regression approach to determining landslide susceptibility in eastern Kentucky, USA: Quarterly Journal of Engineering Geology and Hydrogeology, v. 54, no. 4, article qjegh2020-177, https://doi.org/10.1144/qjegh2020-177.

Crawford, M.M., Koch, H.J., Dortch, J.M., and Haneberg, W.C., 2019, Comparison of LiDAR based landslide hazard assessments for eastern Kentucky [abs.]: American Geophysical Union, AGU Fall Meeting, December 9–13, 2019, San Francisco, CA.

Crawford, M.M., Wang, Z., Carpenter, S., Schmidt, J., Koch, H.J., and Dortch, J.M., 2023, Reconnaissance of landslides and debris flows associated with the July 2022 flooding in eastern Kentucky: Kentucky Geological Survey, ser. 13, Report of Investigations 13, 14 p., https://doi.org/10.13023/kgs.ri56.13.

Crozier, M.J., and Glade, T., 2005, Landslide hazard and risk: Issues, concepts and approach, *in* Glade, T., Anderson, M., and Crozier, M.J., eds., Landslide hazard and risk: Chichester, United Kingdom, Wiley, p. 1–40, https://doi.org/10.1002/9780470012659.ch1.

Dai, C., and Lei, G.H., 2025, Seepage and stability analysis of hydraulically anisotropic unsaturated infinite slopes under steady infiltration: Engineering Geology, v. 344, article 107838, https://doi.org/10.1016/j.enggeo.2024.107838.

Das, B.M., 2010, Principles of geotechnical engineering [7th ed.]: Stamford, CT, Cengage Learning, 666 p.

Dewitz, J., and U.S. Geological Survey, 2021, National Land Cover Database (NLCD) 2019 products [ver. 3, 2024-02]: U.S. Geological Survey, data release, https://doi.org/10.5066/P9KZCM54.

Federal Geographic Data Committee Vegetation Subcommittee (FGDC), 2008, National Vegetation Classification Standard, version 2: Reston, VA, Federal Geographic Data Committee, FGDC-STD-005-2008, 119 p.

Formetta, G., Rago, V., Capparelli, G., Rigon, R., Muto, F., and Versace, P., 2014, Integrated physically based system for modeling landslide susceptibility: Procedia Earth and Planetary Science, v. 9, p. 74–82, https://doi.org/10.1016/j.proeps.2014.06.006.

Greb, S.F., Chesnut, D.R., Jr., Eble, C.F., and Blake, B.M., 2009, The Pennsylvanian of the Appalachian Basin, *in* Greb, S.F., and Chesnut, D.R., Jr., eds., Carboniferous geology and biostratigraphy of the Appalachian Basin: Kentucky Geological Survey, ser. 12, Special Publication 10, p. 32–45.

Hamel, J.V., 1980, Geology and slope stability in western Pennsylvania: Environmental & Engineering Geoscience, v. 17, no. 1, p. 1–26, https://doi.org/10.2113/gseegeosci.xvii.1.1.

Hammond, C., Hall, D., Miller, S., and Swetik, P., 1992, Level I Stability Analysis (LISA) documentation for version 2.0: Ogden, UT, U.S. Department of Agriculture, Forest Service, Intermountain Research Station, General Technical Report INT-285, 190 p.

Haneberg, W.C., 2000, Deterministic and probabilistic approaches to geologic hazard assessment: Environmental & Engineering Geoscience, v. 6, no. 3, p. 209–226, https://doi.org/10.2113/gseegeosci.6.3.209.

Haneberg, W.C., 2004, A rational probabilistic method for spatially distributed landslide hazard assessment: Environmental & Engineering Geoscience, v. 10, no. 1, p. 27–43, https://doi.org/10.2113/10.1.27.

Haneberg, W.C., 2007, PISA-m: probabilistic infinite slope analysis, version 1.0.1 user manual: Seattle, WA, Haneberg Geoscience.

Haneberg, W.C., 2012, Spatially distributed probalistic assessment of submarine slope stability, *in* Allan, P., Arthur, J., Barwise, A., Carrington, T., Cook, M., Hobbs, R., Osborne, J., Powell, T., Salisbury, R., and des Vallières, T., eds., Proceedings of the 7th International Offshore Site Investigation and Geotechnics Conference, London, September 12–14, 2012: London, Society for Underwater Technology, p. 551–556.

Haneberg, W.C., 2015, Understanding the element of time in probabilistic submarine slope stability analyses, in Meyer, V., ed., Frontiers in offshore geotechnics III: Leiden, Netherlands, CRC Press, v. 1, p. 963–968.

Haneberg, W.C., 2016, Incorporating correlated variables into GIS-based probabilistic submarine slope stability assessments, in Lamarche, G., Mountjoy, J., Bull, S., Hubble, T., Krastel, S., Lane, E., Micallef, A., Moscardelli, L., Mueller, C., Pecher, I., and Woelz, S., eds., Submarine mass movements and their consequences: Cham, Switzerland, Springer, p. 529–536, https://doi.org/10.1007/978-3-319-20979-1_53.

Haneberg, W.C., Cole, W.F., and Kasali, G., 2009, High-resolution lidar-based landslide hazard mapping and modeling, UCSF Parnassus Campus, San Francisco, USA: Bulletin of Engineering Geology

and the Environment, v. 68, p. 263–276, https://doi.org/10.1007/s10064-009-0204-3.

Haneberg, W.C., and Gökce, A.Ö., 1994, Rapid water-level fluctuations in a thin colluvium landslide west of Cincinnati, Ohio: U.S. Geological Survey, Bulletin 2059-C, 16 p., https://doi.org/10.3133/b2059C.

Heidemann, H.K., 2012, Lidar base specification [ver. 1.3, 2018-02]: U.S. Geological Survey, Techniques and Methods 11-B4, 101 p., https://doi.org/10.3133/tm11B4.

Hu, Q., Zhou, Y., Wang, S., and Wang, F., 2020, Machine learning and fractal theory models for landslide susceptibility mapping: Case study from the Jinsha River Basin: Geomorphology, v. 351, article 106975, https://doi.org/10.1016/j.geomorph.2019.106975.

Jasiewicz, J., and Stepinski, T.F., 2013, Geomorphons — a pattern recognition approach to classification and mapping of landforms: Geomorphology, v. 182, p. 147–156, https://doi.org/10.1016/j.geomorph.2012.11.005.

Kalpić, D., Hlupić, N., and Lovrić, M., 2011, Student's t-tests, *in* Lovrić, M., ed., International encyclopedia of statistical science: Berlin, Germany, Springer, p. 1559–1563, https://doi.org/10.1007/978-3-642-04898-2_641.

Khabiri, S., Crawford, M.M., Koch, H.J., Haneberg, W.C., and Zhu, Y., 2023, An assessment of negative samples and model structures in landslide susceptibility characterization based on Bayesian network models: Remote Sensing, v. 15, no. 12, article 3200, https://doi.org/10.3390/rs15123200.

McDowell, R.C., 1986, The geology of Kentucky—A text to accompany the geologic map of Kentucky: U.S. Geological Survey, Professional Paper 1151-H, https://doi.org/10.3133/pp1151H.

Montgomery, D.R., and Dietrich, W.E., 1994, A physically based model for the topographic control on shallow landsliding: Water Resources Research, v. 30, no. 4, p. 1153–1171, https://doi.org/10.1029/93WR02979.

National Weather Service (NWS), 2023, Historic July 26th–July 30th, 2022 eastern Kentucky flooding: National Weather Service, https://www.weather.gov/jkl/July2022Flooding [accessed 07/15/2024].

Natural Resources Conservation Service (NRCS), 2023, Soil Survey Geographic (SSURGO) Database: United States Department of Agriculture, https://sdmdataaccess.sc.egov.usda.gov [accessed 09/18/2023].

Newmark, N.M., 1959, A method of computation for structural dynamics: Journal of the Engineering Mechanics Division, v. 85, no. 3, https://doi.org/10.1061/JMCEA3.0000098.

Outerbridge, W.F., 1987, Relation between landslides and bedrock in the central Appalachian Plateaus, *in* Schultz, A.P., and Southworth, C.S., eds., Landslides of eastern North America: U.S. Geological Survey, Circular 1008, p. 36–37, https://doi.org/10.3133/cir1008.

Overfield, B.L., Carey, D.I., Weisenfluh, G.A., Wang, R., and Crawford, M.M., 2015, The geologic context of landslide and rockfall maintenance costs in Kentucky: Kentucky Geological Survey, ser. 12, Report of Investigations 34, 54 p., https://doi.org/10.13023/kgs.ri34.12.

Pack, R.T., Tarboton, D.G., and Goodwin, C.N., 1998, The SINMAP approach to terrain stability mapping, *in* Moore, D., and Hungr, O., eds., Proceedings: Eighth International Congress, International Association for Engineering Geology and the Environment: Rotterdam, Netherlands, Balkema, v. 2, p. 1157–1166.

Parker, R.N., Hales, T.C., Mudd, S.M., Grieve, S.W.D., and Constantine, J.A., 2016, Colluvium supply in humid regions limits the frequency of storm-triggered landslides: Scientific Reports, v. 6, article 34438, https://doi.org/10.1038/srep34438.

Powers, D.M.W., 2001, Evaluation: From precision, recall and F-measure to ROC, informedness, markedness & correlation: Journal of Machine Learning Technologies, v. 2, no. 1, p. 37–63, https://doi.org/10.9735/2229-3981.

PRISM Climate Group, 2024, Annual rainfall averages for subsets of Magoffin and Perry Counties, eastern Kentucky (data created September 13, 2024): Oregon State University, https://prism.oregonstate.edu [accessed 09/13/2024].

Reichenbach, P., Rossi, M., Malamud, B.D., Mihir, M., and Guzzetti, F., 2018, A review of statistically-based landslide susceptibility models: Earth-Science Reviews, v. 180, p. 60–91, https://doi.org/10.1016/j.earscirev.2018.03.001.

Sidle, R.C., and Wu, W., 1999, Simulating effects of timber harvesting on the temporal and spatial distribution of shallow landslides: Zeitschrift für Geomorphologie, v. 43, no. 2, p. 185–201, https://doi.org/10.1127/zfg/43/1999/185.

Sidle, R.C., Pearce, A.J., and O'Loughlin, C.L., 1985, Hillslope stability and land use: Washington, DC, American Geophysical Union, Water Resources Monograph 11, https://doi.org/10.1029/WM011.

Simons, D.B., Li, R.M., and Ward, T.J., 1978, Mapping of potential landslide areas in terms of slope stability: Fort Collins, Colorado State University, Engineering Research Center, prepared for the U.S. Department of Agriculture, Forest Service, Rocky Mountain Forest and Range Experiment Station, rep. CER78-79DBS-RML-TJW19, 75 p.

Soeters, R., and Westen, C.J. van, 1996, Slope instability recognition, analysis, and zonation, *in* Turner, A.K., and Schuster, R.L., eds., Landslides: Investigation and mitigation: Washington, DC, National Academy of Sciences, Transportation Research Board Special Report 247, p. 129–177.

Stillwater Sciences, 2007, Landslide hazard in the Elk River Basin, Humboldt County, California: Arcata, CA, Stillwater Sciences, final report to the North Coast Regional Water Quality Control Board, 51 p., https://www.waterboards.ca.gov/northcoast/water_issues/programs/tmdls/elk_river/pdf/070618/elk_river_landslide_hazards_final%20report.pdf.

Swallom, M.L., Koch, H.J., Dortch, J.M., Crawford, M.M., Thigpen, J.R., and Andrews, W.M., 2025, Evaluating root strength index as an indicator of landslide-prone slopes in eastern Kentucky: Landslides, v. 22, p. 567–578, https://doi.org/10.1007/s10346-024-02384-9.

Ting, K.M., 2017, Confusion matrix, *in* Sammut, C., and Webb, G.I., eds., Encyclopedia of machine learning and data mining [2nd ed.]: New York, Springer, p. 260, https://doi.org/10.1007/978-1-4899-7687-1_50.

Weppner, E., Hoyt, J., and Haneberg, W.C., 2008, Slope stability modeling and landslide hazard in Freshwater Creek and Ryan Slough, Humboldt County, California: Pacific Watershed Associates, prepared for North Coast Regional Water Quality Control Board, report no. 08076901, 69 p., https://www.waterboards.ca.gov/northcoast/water_issues/programs/tmdls/freshwater_creek/pdf/final_reportFresh_modeling_2.pdf.

Wu, W., and Sidle, R.C., 1995, A distributed slope stability model for steep forested basins: Water Resources Research, v. 31, no. 8, p. 2097–2110, https://doi.org/10.1029/95WR01136.

Zhou, C., Wang, Y., Cao, Y., Singh, R.P., Ahmed, B., Motagh, M., Wang, Y., Chen, L., Tan, G., and Li, S., 2024, Enhancing landslide susceptibility modelling through a novel non-landslide sampling method and ensemble learning technique: Geocarto International, v. 39, no. 1, article 2327463, https://doi.org/10.1080/10106049.2024.2327463.